



1 **Analysing surface energy balance closure and partitioning**  
2 **over a semi-arid savanna FLUXNET site in Skukuza, Kruger**  
3 **National Park, South Africa**  
4

5 Nobuhle P. Majazi<sup>1,2</sup>, Chris M. Mannaerts<sup>2</sup>, Abel Ramoelo<sup>1,5</sup>, Renaud Mathieu<sup>1,3</sup>, Alecia  
6 Nickless<sup>4</sup>, Wouter Verhoef<sup>2</sup>

7 <sup>1</sup>Earth Observation Group, Natural Resources and Environment, Council for Scientific and Industrial Research,  
8 Pretoria, South Africa, 0001

9 <sup>2</sup>Department of Water Resources, Faculty of Geo-Information Science and Earth Observation (ITC), University  
10 of Twente, Enschede, 75AA, the Netherlands

11 <sup>3</sup>Department of Geography, Geoinformatics and Meteorology, University of Pretoria, South Africa

12 <sup>4</sup>Nuffield Department of Primary Care Health Sciences, University of Oxford, Oxford, OX2 6GG, United  
13 Kingdom

14 <sup>5</sup>University of Limpopo, Risk and Vulnerability Centre, Sovenga, South Africa, 0727

15 Correspondence to: N. P. Majazi ([nmajazi@csir.co.za](mailto:nmajazi@csir.co.za))  
16

17 **Abstract**

18 Flux towers provide essential terrestrial climate, water and radiation budget information needed for environmental  
19 monitoring and evaluation of climate change impacts on ecosystems and society in general. They are also intended  
20 for calibration and validation of satellite-based earth observation and monitoring efforts, such as assessment of  
21 evapotranspiration from land and vegetation surfaces using surface energy balance approaches.

22 In this paper, 15 years of Skukuza eddy covariance data, i.e. from 2000 to 2014, were analysed for surface  
23 energy balance closure (EBC) and partitioning. The surface energy balance closure was evaluated using the  
24 ordinary least squares regression (OLS) of turbulent energy fluxes (sensible (H) and latent heat (LE)) against  
25 available energy (net radiation (Rn) less soil heat (G)), and the energy balance ratio (EBR). Partitioning of the  
26 surface energy during the wet and dry seasons was investigated, as well as how it is affected by atmospheric vapor  
27 pressure deficit (VPD), and net radiation.

28 After filtering years with bad data (2004-2008), our results show an overall mean EBR of 0.93. Seasonal  
29 variations of EBR also showed summer (0.98) and spring (1.02) were closest to unity, with winter (0.70) having  
30 the least closure. Nocturnal surface energy closure was very low at 0.11, and this was linked to low friction  
31 velocity during night-time, with results showing an increase in closure with increase in friction velocity.

32 The surface energy partitioning of this savanna ecosystem showed that sensible heat flux dominated the  
33 energy partitioning between March and October, followed by latent heat flux, and lastly the soil heat flux, and  
34 during the wet season where latent heat flux dominated the sensible heat flux. An increase in net radiation was  
35 characterized by an increase in both LE and H, with LE showing a higher rate of increase than H in the wet season,  
36 and the reverse happening during the dry season. An increase in VPD is characterized by a decrease in LE and  
37 increase in H during the wet season, and an increase of both fluxes during the dry season.

38  
39 **1. Introduction**

40 Net solar radiation (Rn) reaching the earth's surface determines the amount of energy available for latent (LE),  
41 sensible (H) and soil (G) heat fluxes, and other minor fluxes such as heat stored by the canopy and the ground.  
42 Energy partitioning on the earth's surface is a function of interactions between biogeochemical cycling, plant  
43 physiology, the state of the atmospheric boundary layer and climate (Wilson et al., 2002). How the turbulent  
44 fluxes (H and LE) are partitioned in an ecosystem plays a critical role in determining the hydrological cycle,  
45 boundary layer development, weather and climate (Falge et al., 2005). Understanding the partitioning of energy,  
46 particularly the turbulent fluxes, is important for water resource management in (semi) arid regions, where  
47 potential evapotranspiration far exceeds precipitation.

48 Eddy covariance (EC) systems are currently the most reliable method for measuring carbon, energy and  
49 water fluxes, and they have become a standard technique in the study of surface-atmosphere boundary layer



50 interactions. They provide a distinct contribution to the study of environmental, biological and climatological  
51 controls of the net surface exchanges between the land surface (including vegetation) and the atmosphere  
52 (Aubinet, et al., 1999; Baldocchi et al., 2001). The accuracy of these data is very important because they are used  
53 to validate and assess performance of land surface and climate models. However, the EC techniques have  
54 limitations in terms of data processing and quality control methods, especially under complex conditions (e.g.,  
55 unfavorable weather, such as high turbulence and low wind speed, and heterogeneous topography). In EC  
56 measurements, the ideal situation is that available energy, i.e. net radiation minus soil heat flux is equal to the sum  
57 of the turbulent fluxes ( $Rn-G = LE+H$ ); however, in most instances, the measured available energy is larger than  
58 the sum of the measurable turbulent fluxes of sensible heat and latent heat. Extensive research on the issue of  
59 surface energy imbalance in EC observations has been done (Barr et al., 2012; Chen et al., 2009; Foken et al.,  
60 2010; Franssen et al., 2010; Mauder et al., 2007), and closure error (or imbalance) has been documented to be  
61 around 10-30 %. Causes for non-closure include unaccounted soil and canopy heat storage, non-inclusion of the  
62 low and high frequency turbulence in the computation of the turbulent fluxes, land surface heterogeneities,  
63 systematic measurement and sampling errors. This imbalance has implications on how energy flux measurements  
64 should be interpreted and how these estimates should be compared with model simulations. The surface energy  
65 balance closure is an accepted performance criterion of EC flux data (Twine et al., 2000; Wilson et al., 2002), and  
66 different methods have been used to assess the energy closure and partitioning, including ordinary least squares  
67 regression (OLS) method, i.e. a plot of turbulence fluxes ( $H+LE$ ) against available energy ( $Rn-G$ ), the residual  
68 method, i.e.  $Rn-G-H-LE$ , and the energy balance ratio, i.e.  $LE+H/Rn-G$ .

69 Several researchers have investigated surface energy partitioning and energy balance closure for different  
70 ecosystems, including savannas. Bagayoko et al. (2007) examined the seasonal variation of the energy balance in  
71 West African savannas, and noted that latent heat flux played a major role in the wet season, whereas sensible  
72 heat flux was significant in the dry season. In the grassland Mongolian Plateau, Li et al. (2006) concluded that  
73 sensible heat flux dominated the energy partitioning, followed by ground heat flux, with the rainy season showing  
74 slight increase in latent heat flux. Gu et al. (2006) used different ratios (Bowen ratio,  $G/Rn$ ,  $H/Rn$  and  $LE/Rn$ ) to  
75 investigate surface energy exchange in the Tibetan Plateau, and showed that during the vegetation growth period,  
76  $LE$  was higher than  $H$ , and this was reversed during the post-growth period.

77 Research using the Skukuza EC system data has focused mainly on the carbon exchange, fire regimes, and  
78 in global analysis of the energy balance (Archibald et al., 2009; Kutsch et al., 2008; Williams et al., 2009).  
79 However, there has been no investigation of surface energy partitioning and energy balance closure in this  
80 ecosystem. In this study, we examined the surface energy balance partitioning into soil heat conduction,  
81 convection (sensible) and latent heat components and its energy balance closure using 15 years (2000-2014) of  
82 eddy covariance data from the Skukuza flux tower.

83 First, a multi-year surface energy balance closure (EBC) analysis was done, including the seasonal and day-  
84 night EBC evaluations, and an assessment of its error sources. This included investigating how friction velocity  
85 affects the closure, and its link to low nighttime EBC. Surface energy partitioning during the wet and dry seasons  
86 was examined, including how meteorological conditions such as vapour pressure deficit (VPD) and  $Rn$  affect the  
87 partitioning.



## 88 2. Materials and methods

### 89 2.1. Site description

90 The Skukuza flux tower (25.02°S, 31.50°E) was established early 2000 as part of the SAFARI 2000 campaign  
91 and experiment, set up to understand the interactions between the atmosphere and the land surface in southern  
92 Africa by connecting ground data of carbon, water, and energy fluxes with remote sensing data generated by Earth  
93 observing satellites (Scholes et al., 2001; Shugart et al., 2004).

94 The site is located in the Kruger National Park (South Africa) at 365 m above sea level, and receives 550  
95  $\pm$  160 mm precipitation per annum between November and April, with significant inter-annual variability. The  
96 year is divided into a hot, wet growing season and a warm, dry non-growing season. The soils are generally  
97 shallow, with coarse sandy to sandy loam textures (about 65 % sand, 30 % clay and 5% silt). The area is  
98 characterised by a catenal pattern of soils and vegetation, with broad-leaved *Combretum* savanna on the crests  
99 dominated by the small trees (*Combretum apiculatum*), and fine-leaved *Acacia* savanna in the valleys dominated  
100 by *Acacia nigrescens* (Scholes et al., 1999). The vegetation is mainly open woodland, with approximately 30 %  
101 tree canopy cover of mixed *Acacia* and *Combretum* savanna types. Tree canopy height is 5–8 m with occasional  
102 trees (mostly *Sclerocarya birrea*) reaching 10 m. The grassy and herbaceous understory comprises grasses such  
103 as *Panicum maximum*, *Digitaria eriantha*, *Eragrostis rigidior*, and *Pogonarthria squarrosa*.

104

#### 105 2.1.1. Eddy covariance system

106 Since 2000, ecosystem-level fluxes of water, heat and carbon dioxide are measured using an eddy covariance  
107 system mounted at 16 m height of the 22 m high flux tower. The measurements taken and the instruments used  
108 are summarised in Table 1.

#### 109 (Table 1)

110 From 2000 to 2005, H and LE were derived from a closed-path CO<sub>2</sub>/H<sub>2</sub>O monitoring system, which was replaced  
111 by the open-path gas analyser in 2006. Also, from 2000 to 2008, incident and reflected shortwave radiation (i.e.  
112 300–1100 nm, Wm<sup>-2</sup>), incident and reflected near-infrared (600–1100 nm, Wm<sup>-2</sup>) and incoming and emitted  
113 longwave radiation (>3.0  $\mu$ m, Wm<sup>-2</sup>) measurements were made using a two-component net radiometer (Model  
114 CNR 2: Kipp & Zonen, Delft, The Netherlands) at 20 s intervals and then recorded in the data-logger as 30 min  
115 averages; this was replaced with the Kipp & Zonen NRLite net radiometer in 2009. Soil heat flux is measured  
116 using the HFT3 plates (Campbell Scientific) installed at 5 cm below the surface at three locations, two under tree  
117 canopies and one between canopies.

118 Ancillary meteorological measurements include air temperature and relative humidity, also measured at  
119 16 m height, using a Campbell Scientific HMP50 probe; precipitation at the top of the tower using a Texas  
120 TR525M tipping bucket rain gauge; wind speed and direction using a Climatronics Wind Sensor; and soil  
121 temperature using Campbell Scientific 107 soil temperature probe.

122

#### 123 2.1.2. Data pre-processing

124 Post-processing of the raw high frequency (10 Hz) data for calculation of half-hour periods of the turbulent fluxes  
125 and CO<sub>2</sub> ( $F_c$ ; g CO<sub>2</sub> m<sup>-2</sup> time<sup>-1</sup>) involved standard spike filtering, planar rotation of velocities and lag correction  
126 to CO<sub>2</sub> and q (Aubinet et al., 1999; Wilczak et al., 2001). All fluxes are reported as positive upward from the land  
127 to the atmosphere. Frequency response correction of some of the energy lost due to instrument separation, tube



128 attenuation, and gas analyzer response for LE and  $F_c$  was performed with empirical co-spectral adjustment to  
129 match the H co-spectrum (Eugster and Senn, 1995; Su et al., 2004).

130

## 131 2.2. Data analysis

132 Half-hourly measurements of eddy covariance and climatological data from 2000 to 2014 were used to assess  
133 surface energy partitioning and closure. Screening of the half-hourly data rejected i) data from periods of sensor  
134 malfunction (i.e. when there was a faulty diagnostic signal), (ii) incomplete 30-minute datasets of Rn, G, LE and  
135 H, and (iii) outliers. After data screening, flux data with non-missing values of Rn, G, LE and H data were arranged  
136 according to monthly and seasonal periods (summer (December – February), autumn (March – May), winter (June  
137 – August), and spring (September – November)), as well as into daytime and nighttime.

138

### 139 2.2.1. Surface energy balance assessment

140 The law of conservation of energy states that energy can neither be created nor destroyed, but is transformed from  
141 one form to another, hence the ideal surface energy balance equation is written as:

$$142 \quad Rn - G = H + LE \quad (1)$$

143 Energy imbalance occurs when both sides of the equation do not balance. The energy balance closure was  
144 evaluated at different levels, i.e. multi-year, seasonal, and day/ night periods (the assumption being that daytime  
145 has positive Rn and nighttime has negative Rn), using two methods, i.e.

146 i) The ordinary least squares method (OLS), which is the regression between turbulent fluxes and available  
147 energy.

148 Ideal closure is when the intercept is zero and slope and the coefficient of determination are one. An assumption  
149 is made using this method, that there are no random errors in the independent variables, i.e. Rn and G, which of  
150 course is an incorrect assumption.

151 ii) The energy balance ratio (EBR), which is ratio of the sum of turbulent fluxes to the available energy,

$$152 \quad \frac{\sum(LE + H)}{\sum(Rn - G)}.$$

153 The EBR gives an overall evaluation of energy balance closure at longer time scales by averaging over errors in  
154 the half-hour measurements; and the ideal closure is 1. EBR has the potential to remove biases in the half-hourly  
155 data, such as the tendency to overestimate positive fluxes during the day and underestimate negative fluxes at  
156 night.

157 To investigate the effect of friction velocity on EBR and how it is related to time of day, using friction  
158 velocity, the data were separated into 4 25-percentiles, and the EBR and OLS evaluated.

159

### 160 2.2.2. Analyzing surface energy partitioning

161 To evaluate solar radiation variation and partitioning into latent and sensible heat fluxes in this biome, EC surface  
162 energy data from 2000 to 2014 were used. The data gaps in these data were first filled using the Amelia II software  
163 (Honaker et al., 2011). This R-program was designed to impute missing data using a bootstrapping-based multiple  
164 imputation algorithm. The minimum, maximum and mean statistics of Rn, H, LE and G were then estimated.

165 The monthly and seasonal variations of energy partitioning were assessed. Surface energy partitioning  
166 was also characterized as a direct function of vapor pressure deficit (VPD) and Rn during the wet and dry seasons.

167



168 **3. Results and discussion**

169 **3.1. Meteorological conditions**

170 Fig 1 shows the 15-year average daily temperature, VPD and rainfall totals at the Skukuza flux tower. The annual  
171 average temperatures over the 15-year period ranged between 21.13°C in 2012 and 23.23 °C in 2003, with a 15-  
172 year average temperature of 22.9 °C. While 2003 was the hottest year, it was also the driest year, with annual  
173 rainfall of 273.6 mm, with 2002 also recording very low rainfall of 325.4 mm, both receiving rainfall amounts  
174 below the recorded mean annual rainfall of 550±160 mm. The wettest years were 2013, 2000, 2014 and 2004  
175 which received 1414, 1115.6, 1010.2 and 1005.7 mm, respectively. 2007 and 2008 had incomplete rainfall data  
176 records to assess their annuals. The annual daily average VPD was between 0.024 and 4.03 kPa, with an overall  
177 average of  $1.28 \pm 0.62$  kPa. The daily average VPD decreased with rainy days, and showed an increase during  
178 rain-free days. The wet years, i.e. 2000, 2013 and 2014 had low annual average VPD of 1.98, 1.34 and 1.83 kPa,  
179 respectively, whereas the drought years exhibited high VPDs with 2002 and 2003 with 2.77 and 2.97 kPa,  
180 respectively. The long-term weather records are comparable with the 1912 – 2001 and 1960 – 1999 climate  
181 analysis for the same area as reported by Kruger et al. (2002) and Scholes et al. (2001), showing a mean annual  
182 total precipitation of 547.1 mm and air temperature of 21.9 °C. The low rainfall during 2000-2003 seasons was  
183 also reported by Kutch et al. (2008), who were investigating the connection between water relations and carbon  
184 fluxes during the mentioned period.

185 **(Figure 1)**

186

187 **3.2. Surface energy balance assessment**

188 Data completeness varied largely 3.24 % (2013) and 57.65 % (2010), with a mean of 30.77 %. The variation in  
189 data completeness is due to a number of factors including instrument failures, changes and (re)calibration, and  
190 poor weather conditions.

191

192 **3.2.1. Multi-year analysis of surface energy balance closure**

193 Fig 2 summarizes results of the multi-year energy balance closure analysis for the Skukuza eddy covariance  
194 system from 2000 to 2014. The slopes ranged between 0.93 and 1.47, with a mean 1.19 with standard deviation  
195 of 0.21, and the intercepts were a mean of 17.79 with standard deviation of 32.96 Wm<sup>-2</sup>. R<sup>2</sup> ranged between 0.73  
196 in 2005 and 0.92 in 2003, with a mean of 0.86 with standard deviation of 0.05.

197 The annual energy balance ratio (EBR) for the 15 years ranged between 0.44 in 2007 and an extreme  
198 3.76 in 2013, with a mean of  $0.97 \pm 0.81$ . Between 2004 and 2008, EBR ranges between 0.44 and 0.53, whereas  
199 from 2000 to 2003 and 2009 to 2014, the EBR ranged 0.76 and 1.09. The EBR for 2010 to 2012 were slightly  
200 greater than 1, indicating an overestimation of the turbulent fluxes (H+LE) compared to the available energy. The  
201 remaining years were less than 1, indicating that the turbulent fluxes were lower than the available energy. The  
202 period of low EBR between 2004 and 2008 is characterized by the absence of negative values of available energy  
203 (Rn-G) as illustrated in Fig 2. Between 2000 and 2004, the CNR2 net radiometer was used to measure long and  
204 shortwave radiation, and these were combined to derive Rn. However, when the pyrgeometer broke down in 2004,  
205 Rn was derived from measured shortwave radiation and modelled longwave radiation until the CNR2 was  
206 replaced by the NRLite net radiometer in 2009. This was a significant source of error, as shown by the low EBR  
207 between 2004 and 2008. The closed-path gas analyzer was also changed to open-path gas analyzer in 2006. An



208 analysis of the 2006 data (which had very low data completeness of 7.59 %) showed that there were no  
209 measurements recorded until September, possibly due to instrument failure. Our final proposed mean multiyear  
210 EBR estimate for the 15-year period (2000-2014), excluding the years with data issues (2004 to 2008, and 2013),  
211 was therefore  $0.93 \pm 0.11$ . For further analysis of the EBR, we excluded the years with bad data.

#### 212 (Figure 2)

213 The EBR results for the Skukuza eddy covariance system, with a mean of 0.93 (only the years with good data),  
214 are generally within the reported accuracies by most studies that report the energy balance closure error at 10 –  
215 30%. Chen et al. (2009) report a mean of 0.98 EBR, average slope of 0.83, and  $R^2$  ranges between 0.87 and 0.94  
216 for their study in the semi-arid region of Mongolia. Wilson et al., (2002) also reported that the mean annual EBR  
217 for 22 FLUXNET sites was 0.84, ranging from 0.34 to 1.69, and slopes and intercepts ranging from 0.53 to 0.99,  
218 and from  $-33$  to  $37 \text{ W m}^{-2}$ , respectively. Yuling et al. (2005) also report that in the ChinaFLUX, EBR ranged  
219 between 0.58 and 1.00, with a mean of 0.83. von Randow et al. (2004) showed an energy imbalance of 26 % even  
220 after correcting for the angle of attack on the sonic anemometer in the forested Jeru study area in the Amazon,  
221 and explained this as due to either slow wind direction changes which result in low frequency components that  
222 cannot be captured using short time rotation scales, and the difficulty in estimating horizontal flux divergences  
223 caused by energy that is transported horizontally by circulations. Sanchez et al., (2010) showed that the inclusion  
224 of the storage term in the EBR improved the closure by almost 6 % from 0.72, in their study in a FLUXNET  
225 boreal site in Finland. Using data from the Tibetan Observation and Research Platform (TORP), Liu et al. (2011)  
226 observed an EBR value of 0.85 in an alfalfa field in semi-arid China. Also under similar semi-arid conditions, in  
227 China, an EBR value of 0.80 was found by Xin and Liu (2010) in a maize crop. Were et al. (2007) reported EBR  
228 values of about 0.90 over shrub and herbaceous patches, in a dry valley in southeast Spain.

229

#### 230 3.2.2. Seasonal variation of EBR

231 Fig 3 shows the seasonal OLS results for the 15 year period, excluding years 2004 to 2008 and 2013. The slopes  
232 ranged between 0.94 and 1.21, with a mean of  $1.10 \pm 0.11$ , and the intercepts were a mean of  $11.97 \text{ Wm}^{-2} \pm 3.87$   
233  $\text{Wm}^{-2}$ .  $R^2$  ranged between 0.74 and 0.88 with a mean of  $0.83 \pm 0.06$ . The EBR for the different seasons ranged  
234 between 0.70 and 1.02, with a mean of  $0.88 \pm 0.14$ . The winter season had the lowest EBR of 0.70, while summer  
235 and spring were closest to unity with EBR of 0.98 and 1.02, respectively, and autumn had EBR of 0.84. A large  
236 number of outliers is observed in summer due to cloudy weather conditions and rainfall events that make the  
237 thermopile surface wet, thus reducing the accuracy of the net radiometer. A study comparing different the  
238 performance of different net radiometers by Blonquist et al. (2009) shows that the NR-Lite is highly sensitive to  
239 precipitation and dew/ frost since it the sensor is not protected.

#### 240 (Figure 3)

241 Wilson et al. (2002) comprehensively investigated the energy closure of the summer and winter seasons for 22  
242 FLUXNET sites for 50 site-years. They also reported higher energy balance correlation during the wet compared  
243 to the dry season, with the mean  $R^2$  of 0.89 and 0.68, respectively. However, their EBR showed smaller differences  
244 between the two seasons, being 0.81 and 0.72, for summer and winter, respectively, whereas for Skukuza, the  
245 differences were much significant. Ma et al. (2009) reported an opposite result from the Skukuza results, showing  
246 energy closures of 0.70 in summer and 0.92 in winter over the flat prairie on the northern Tibetan Plateau.

247



### 248 3.2.3. Day – night-time effects

249 Fig 4 shows the daytime and nocturnal OLS regression results for the 15 year period. The daytime and nocturnal  
250 slopes were 0.99 and 0.11, with the intercepts being 76.76 and 1.74  $\text{Wm}^{-2}$ , respectively. Daytime and nocturnal  
251  $R^2$  were 0.64 and 0.01, respectively. The EBR for the different times of day were 0.96 and 0.27, daytime and  
252 nocturnal, respectively.

#### 253 (Figure 4)

254 Other studies also reported a higher daytime surface energy balance closure. For instance, Wilson et al., (2002)  
255 showed that the mean annual daytime EBR was 0.8, whereas the nocturnal EBR was reported to be negative  
256 or was much less or much greater than 1.

257 To understand the effect of friction velocity on the energy balance closure, which had friction velocity  
258 ( $u_*$ ) data, were used. Using friction velocity, the data were separated into 4 25-percentiles, and the EBR and OLS  
259 evaluated. Results show that the first quartile, the EBR was 3.94, with the 50-percentile at 0.99, the third quartile  
260 at unity, and the fourth quartile at 1.03 (Fig 5). The slopes were between 1.01 and 1.12, with the intercepts ranging  
261 between -9.26 and -0.17  $\text{Wm}^{-2}$ , whereas  $R^2$  were 0.82, 0.86, 0.85 and 0.81 for the first to the fourth quartiles,  
262 respectively.

#### 263 (Figure 5)

264 A quick assessment shows that the time associated with the low friction velocities, i.e. the first quartile are night-  
265 time data constituting 81 % of the whole first quartile dataset, and the last quartile had the highest number of  
266 daytime values at 79.29 % of the fourth quartile dataset. Lee and Hu (2002) hypothesized that the lack of energy  
267 balance closure during nocturnal periods was often the result of mean vertical advection, whereas Aubinet et al.,  
268 (1999) and Blanken et al., (1997) showed that energy imbalance during nocturnal periods is usually greatest when  
269 friction velocity is small. Another source of error in the nocturnal EBR is the high uncertainty in night-time  
270 measurements of  $R_n$ . At night, the assumption is that there is no shortwave radiation, and  $R_n$  is a product of  
271 longwave radiation. Studies show that night-time measurements of longwave radiation were less accurate than  
272 daytime measurements (Blonquist et al., 2009). The RN-Lite, for instance has low sensitivity to longwave  
273 radiation, resulting in low accuracy in low measurements.

274

## 275 3.3. Surface energy partitioning

### 276 3.3.1. Surface energy measurements

277 The mean daily and annual measurements of the energy budget components from 2000 to 2014 are highlighted in  
278 Fig 6 and Table 2. The seasonal cycle of each component can be seen throughout the years, where at the beginning  
279 of each year the energy budget components are high, and as each year progresses they all decrease to reach a low  
280 during the middle of the year, which is the winter/ dry season, and a gradual increase being experienced during  
281 spring right to the summer at the end of each year. The multi-year daily means of  $R_n$ , H, LE and G were 139.1  
282  $\text{Wm}^{-2}$ , 57.70  $\text{Wm}^{-2}$ , 42.81  $\text{Wm}^{-2}$  and 2.94  $\text{Wm}^{-2}$ , with standard deviations of 239.75  $\text{Wm}^{-2}$ , 104.15  $\text{Wm}^{-2}$ , 70.58  
283  $\text{Wm}^{-2}$  and 53.67  $\text{Wm}^{-2}$ , respectively.

#### 284 (Figure 6)

285 The gaps in 2006 and 2013 indicates the absence of the surface energy flux measurements in those years, which  
286 was a result of instrument failure. Between 2004 and 2008, the  $R_n$  was calculated as a product of measured



287 shortwave radiation and modelled longwave radiation, which was a high source of error in the estimation of Rn.  
288 These years are also characterised by poor energy balance closure, as shown in Section 3.2.1 above.

289 (Table 2)

290

### 291 3.3.2. Influence of weather conditions and seasonality

292 In arid/semi-arid ecosystems, solar radiation is not a limiting factor for evapotranspiration, instead it is mainly  
293 limited by water availability. The seasonal fluctuations of energy fluxes are affected by the seasonal changes in  
294 the solar radiation, air temperature, precipitation and soil moisture (Baldocchi et al., 2000; Arain et al., 2003).  
295 These climatic variables influence vegetation dynamics in an ecosystem, as well as how solar radiation is  
296 partitioned. Hence, daily measurements of precipitation, air temperature and VPD were evaluated to investigate  
297 the partitioning of the surface energy in the semi-arid savanna landscape of Skukuza.)

298 (Figure 7)

299 To illustrate the partitioning of solar radiation into the different fluxes throughout the year, Fig 7 presents  
300 the multi-year mean monthly variations of the surface energy components showing a general decrease of the  
301 components between February and June, which then gradually increases again until November. The multi-year  
302 monthly means of Rn, H, LE and G were 71.27 Wm<sup>-2</sup> (June) and 197.33 Wm<sup>-2</sup> (November), 37.11 Wm<sup>-2</sup> (June)  
303 and 80.37 Wm<sup>-2</sup> (November), 8.52 Wm<sup>-2</sup> (August) and 127.17 Wm<sup>-2</sup> (December), -2.28 Wm<sup>-2</sup> (June) and 20.78  
304 Wm<sup>-2</sup> (November), respectively. The month of August had the highest BR of 6.42, whereas December had the  
305 least at 0.42. The residual accounted for between -19.69 and 34.74 % of Rn, and an average of 4.70 %.

306 The general trend shows that sensible heat flux dominated the energy partitioning between May and  
307 October, followed by latent heat flux, and lastly the soil heat flux, except during the wet season where latent heat  
308 flux was larger than sensible heat flux. This is illustrated by the trend of BR, showing an increase of BR from  
309 April, with the peak in August, then a steady decrease until it hits lowest in December. The period of low BR is  
310 characterised by high incoming solar radiation, with high Rn and high precipitation (Fig 1). As the season  
311 transitions into winter, it is characterised by reduced net radiation and low measurements H and LE.

312 Just before the first rains, i.e. between September and November, tree flowering and leaf emergence  
313 occurs in the semi-arid savanna in the Skukuza area (Archibald and Scholes, 2007), and grasses shoot as soil  
314 moisture availability improves with the rains (Scholes et al., 2003). This is characterised by a gradual increase in  
315 latent heat flux (evapotranspiration) and decrease in BR, which, when compared to the winter season, is  
316 significantly lower than the sensible heat flux, as illustrated in Fig 7. As the rainy season progresses, and  
317 vegetation development peaks, latent heat flux also reaches its maximum, becoming significantly higher than  
318 sensible heat flux, and hence, high BR. Between March and September, when leaf senescence occurs, the leaves  
319 gradually change colour to brown and grass to straw, and trees defoliate, sensible heat flux again gradually  
320 becomes significantly higher than LE.

321 The influence of VPD and Rn on surface energy partitioning was investigated during the wet and dry  
322 seasons. Results show that there is an increase in H and decrease in LE with an increase in VPD in the wet season  
323 (Fig 9). As illustrated earlier (Fig 1), VPD is higher when there is little or no rain (low soil water availability),  
324 which explains the increase in H with a rise VPD (Fig 9d). In this instance, although the evaporative demand is  
325 high, the stomatal conductance is reduced due to absence of water in the soil, resulting in smaller LE and higher  
326 H. Rn, on the other hand, is partitioned into different fluxes, based on other climatic and vegetation physiological





327 characteristics. Figure 10 illustrates that both latent and sensible heat flux increase with increase in net radiation,  
328 although their increases are not in proportion, based on season. During the wet season, the rate of increase of LE  
329 is higher than that of H, whereas in the dry season the reverse is true. The rate of increase of LE is controlled by  
330 the availability of soil water (precipitation), (also illustrated in Figures 1c and 6 (LE)), and during the wet season  
331 it increases steadily with increasing Rn, whereas the rate of increase of H is concave, showing saturation with an  
332 increase in Rn. The opposite is true during the dry season, with limited water availability, the rate of increase of  
333 LE slows down with increase in Rn, and a steady increase of H with Rn increase.

334 Gu et al. (2006) examined how soil moisture, vapor pressure deficit (VPD) and net radiation control  
335 surface energy partitioning at a temperate deciduous forest site in central Missouri, USA. They ascertained that  
336 with ample soil moisture, latent heat flux dominates over sensible heat flux, and reduced soil moisture availability  
337 reversed the dominance of latent heat over sensible heat, because of its direct effect on stomatal conductance. An  
338 increase in net radiation, on the other hand, also increases both sensible and latent heat fluxes. The increase of  
339 either then becomes a function of soil moisture availability, since they cannot increase in the same proportion.  
340 Their findings are generally consistent with our results, which show that during the rainy season, latent heat flux  
341 was significantly higher than sensible heat flux, whereas, during the other seasons, sensible heat flux remained  
342 higher than latent heat flux. However, their findings on the effect of VPD on energy partitioning are opposite of  
343 our study, where they record significant increase in LE and decrease in H with a rise in VPD during the non-  
344 drought period; in dry conditions, both components show slight increases with increase in VPD. Li et al. (2012)  
345 also investigated the partitioning of surface energy in the grazing lands of Mongolia, and concluded that the energy  
346 partitioning was also controlled by vegetation dynamics and soil moisture availability, although soil heat flux is  
347 reportedly higher than latent heat flux in most instances. In a temperate mountain grassland in Austria, Hammerle  
348 et al., (2008) found that the energy partitioning in this climatic region was dominated by latent heat flux, followed  
349 by sensible heat flux and lastly soil heat flux.

350 The consensus in all above studies is that vegetation and climate dynamics play a critical role in energy  
351 partitioning. They note that during full vegetation cover, latent heat flux is the dominant portion of net radiation.  
352 However, depending on the climatic region, the limiting factors of energy partitioning vary between water  
353 availability and radiation. Our study confirms that in semi-arid regions, sensible heat flux is the highest fraction  
354 of net radiation throughout the year, except during the wet period, when latent heat flux surpasses sensible heat  
355 flux. However, in regions and locations where water availability is not a limiting factor, latent heat flux may take  
356 the highest portion of net radiation.

357

#### 358 4. Conclusion

359 This study investigated both surface energy balance and its partitioning into turbulent fluxes during the wet and  
360 dry seasons in a semi-arid savanna ecosystem in Skukuza using eddy covariance data from 2000 to 2014. The  
361 analysis revealed a mean multi-year energy balance ratio of 0.93, The variation of RBR based on season, time of  
362 day and as a function of friction velocity was explored. The seasonal EBR varied between 0.70 and 0.88, with  
363 winter recording the highest energy imbalance. Daytime EBR was as high as 0.96, with 0.27 EBR for the  
364 nighttime. The high energy imbalance at night was explained as a result of stable conditions, which limit  
365 turbulence that is essential for the creation of eddies. The assessment of the effect of friction velocity on EBR



366 showed that EBR increased with an increase in friction velocity, with low friction velocity experienced mainly  
367 during night-time.

368 The energy partition analysis revealed that sensible heat flux is the dominant portion of net radiation in  
369 this semi-arid region, except in summer, when there is rainfall. The results also show that water availability and  
370 vegetation dynamics play a critical role in energy partitioning, whereby when it rains, vegetation growth occurs,  
371 leading to an increase in latent heat flux / evapotranspiration. Clearly an increase in  $R_n$  results in a rise in  $H$  and  
372  $LE$ , however their increases are controlled by water availability. During the wet season, the rate of increase of  $LE$   
373 is higher than that of  $H$ , whereas in the dry season the reverse is true. The rate of increase of  $LE$  is controlled by  
374 the availability of soil water (precipitation), and during the wet season it increases steadily with increasing  $R_n$ ,  
375 whereas the rate of increase of  $H$  shows saturation with an increase in  $R_n$ . The opposite is true during the dry  
376 season, with limited water availability, the rate of increase of  $LE$  reaches saturation with increase in  $R_n$  and a  
377 steady increase of  $H$  with  $R_n$  increase. An increase in  $VPD$ , on the other hand, results in an increase in  $H$  and  
378 decrease in  $LE$ , with higher  $VPD$  experienced during the dry season, which explains the high  $H$ , although the  
379 evaporative demand is high.

380

#### 381 **Acknowledgements**

382 This study was supported by the Council for Scientific and Industrial Research under the project entitled  
383 “Monitoring of water availability using geo-spatial data and earth observations”, and the National Research  
384 Foundation under the Thuthuka PhD cycle grant.

385

#### 386 **References**

- 387 Archibald, S., & Scholes, R. (2007). Leaf green-up in a semi-arid african savanna-separating tree and grass  
388 responses to environmental cues. *Journal of Vegetation Science*, 18(4), 583-594.
- 389 Archibald, S., Kirton, A., Merwe, M., Scholes, R., Williams, C., & Hanan, N. (2009). Drivers of inter-annual  
390 variability in net ecosystem exchange in a semi-arid savanna ecosystem, South africa. *Biogeosciences*, 6(2), 251-  
391 266.
- 392 Aubinet, M., Grelle, A., Ibrom, A., Rannik, Ü., Moncrieff, J., Foken, T., . . . Bernhofer, C. (1999). Estimates of  
393 the annual net carbon and water exchange of forests: The EUROFLUX methodology. *Advances in Ecological  
394 Research*, 30, 113-175.
- 395 Bagayoko, F., Yonkeu, S., Elbers, J., & van de Giesen, N. (2007). Energy partitioning over the West African  
396 savanna: Multi-year evaporation and surface conductance measurements in eastern burkina faso. *Journal of  
397 Hydrology*, 334(3), 545-559.
- 398 Baldocchi, D., Falge, E., Gu, L., Olson, R., Hollinger, D., Running, S., . . . Evans, R. (2001). FLUXNET: A new  
399 tool to study the temporal and spatial variability of ecosystem-scale carbon dioxide, water vapor, and energy flux  
400 densities. *Bulletin of the American Meteorological Society*, 82(11), 2415-2434.
- 401 Barr, A. G., van der Kamp, G., Black, T. A., McCaughey, J. H., & Nesic, Z. (2012). Energy balance closure at  
402 the BERMS flux towers in relation to the water balance of the White Gull Creek watershed 1999–2009.  
403 *Agricultural and Forest Meteorology*, 153(0), 3-13.
- 404 Blanken, P., Black, T. A., Yang, P., Neumann, H., Nesic, Z., Staebler, R., . . . Lee, X. (1997). Energy balance and  
405 canopy conductance of a boreal aspen forest: Partitioning overstory and understory components. *Journal of  
406 Geophysical Research: Atmospheres* (1984–2012), 102(D24), 28915-28927.



- 407 Blonquist, J., et al. (2009). "Evaluation of measurement accuracy and comparison of two new and three traditional  
408 net radiometers." *Agricultural and Forest Meteorology* **149**(10): 1709-1721.
- 409 Chen, S., Chen, J., Lin, G., Zhang, W., Miao, H., Wei, L., . . . Han, X. (2009). Energy balance and partition in  
410 inner Mongolia steppe ecosystems with different land use types. *Agricultural and Forest Meteorology*, **149**(11),  
411 1800-1809.
- 412 Eugster, W., & Senn, W. (1995). A cospectral correction model for measurement of turbulent NO<sub>2</sub> flux. *Boundary-  
413 Layer Meteorology*, **74**(4), 321-340.
- 414 Falge, E., Reth, S., Brüggemann, N., Butterbach-Bahl, K., Goldberg, V., Oltchev, A., . . . Queck, R. (2005).  
415 Comparison of surface energy exchange models with eddy flux data in forest and grassland ecosystems of  
416 germany. *Ecological Modelling*, **188**(2), 174-216.
- 417 Foken, T., Mauder, M., Liebethal, C., Wimmer, F., Beyrich, F., Leps, J., . . . Bange, J. (2010). Energy balance  
418 closure for the LITFASS-2003 experiment. *Theoretical and Applied Climatology*, **101**(1-2), 149-160.
- 419 Franssen, H., Stöckli, R., Lehner, I., Rotenberg, E., & Seneviratne, S. (2010). Energy balance closure of eddy-  
420 covariance data: A multisite analysis for european FLUXNET stations. *Agricultural and Forest Meteorology*,  
421 **150**(12), 1553-1567.
- 422 Goosse H., P.Y. Barriat, W. Lefebvre, M.F. Loutre and V. Zunz, (2008-2010). Introduction to climate dynamics  
423 and climate modeling. Online textbook available at <http://www.climate.be/textbook>.
- 424 Gu, L., Meyers, T., Pallardy, S. G., Hanson, P. J., Yang, B., Heuer, M., . . . Wullschleger, S. D. (2006). Direct  
425 and indirect effects of atmospheric conditions and soil moisture on surface energy partitioning revealed by a  
426 prolonged drought at a temperate forest site. *Journal of Geophysical Research: Atmospheres* (1984–2012),  
427 **111**(D16)
- 428 Hammerle, A., Haslwanter, A., Tappeiner, U., Cernusca, A., & Wohlfahrt, G. (2008). Leaf area controls on energy  
429 partitioning of a temperate mountain grassland. *Biogeosciences (Online)*, **5**(2).
- 430 Honaker, J., et al. (2011). "Amelia II: A program for missing data." *Journal of statistical software* **45**(7): 1-47.
- 431 Kutsch, W., Hanan, N., Scholes, R., McHugh, I., Kubheka, W., Eckhardt, H., & Williams, C. (2008). Response  
432 of carbon fluxes to water relations in a savanna ecosystem in south africa. *Biogeosciences Discussions*, **5**(3),  
433 2197-2235.
- 434 Li, J., Zhang, B., Shen, Q., Zou, L., & Li, L. (2012). Monitoring water quality of lake taihu from HJ-CCD data  
435 using empirical models. Paper presented at the Geoscience and Remote Sensing Symposium (IGARSS), 2012  
436 IEEE International, 812-815.
- 437 Li, S., Eugster, W., Asanuma, J., Kotani, A., Davaa, G., Oyunbaatar, D., & Sugita, M. (2006). Energy partitioning  
438 and its biophysical controls above a grazing steppe in central mongolia. *Agricultural and Forest Meteorology*,  
439 **137**(1), 89-106.
- 440 Liu, S., Xu, Z., Wang, W., Jia, Z., Zhu, M., Bai, J., & Wang, J. (2011). A comparison of eddy-covariance and  
441 large aperture scintillometer measurements with respect to the energy balance closure problem. *Hydrology and  
442 Earth System Sciences*, **15**(4), 1291-1306.
- 443 Ma, Y., Wang, Y., Wu, R., Hu, Z., Yang, K., Li, M., . . . Chen, X. (2009). Recent advances on the study of  
444 atmosphere-land interaction observations on the tibetan plateau. *Hydrology and Earth System Sciences*, **13**(7),  
445 1103-1111.



- 446 Mauder, M., Jegede, O., Okogbue, E., Wimmer, F., & Foken, T. (2007). Surface energy balance measurements at  
447 a tropical site in west africa during the transition from dry to wet season. *Theoretical and Applied Climatology*,  
448 89(3-4), 171-183.
- 449 Sánchez, J., Caselles, V., & Rubio, E. (2010). Analysis of the energy balance closure over a FLUXNET boreal  
450 forest in finland. *Hydrology and Earth System Sciences*, 14(8), 1487-1497.
- 451 Scholes, R., Gureja, N., Giannecchini, M., Dovie, D., Wilson, B., Davidson, N., . . . Freeman, A. (2001). The  
452 environment and vegetation of the flux measurement site near skukuza, kruger national park. *Koedoe-African*  
453 *Protected Area Conservation and Science*, 44(1), 73-83.
- 454 Scholes, R. J., Bond, W. J., & Eckhardt, H. C. (2003). *Vegetation dynamics in the kruger ecosystem The Kruger*  
455 *Experience*. Island Press.
- 456 Shugart, H., Macko, S., Lesolle, P., Szuba, T., Mukelabai, M., Dowty, P., & Swap, R. (2004). The SAFARI 2000–  
457 Kalahari transect wet season campaign of year 2000. *Global Change Biology*, 10(3), 273-280.
- 458 Su, H., Schmid, H. P., Grimmond, C., Vogel, C. S., & Oliphant, A. J. (2004). Spectral characteristics and  
459 correction of long-term eddy-covariance measurements over two mixed hardwood forests in non-flat terrain.  
460 *Boundary-Layer Meteorology*, 110(2), 213-253.
- 461 Twine, T. E., Kustas, W., Norman, J., Cook, D., Houser, P., Meyers, T., . . . Wesely, M. (2000). Correcting eddy-  
462 covariance flux underestimates over a grassland. *Agricultural and Forest Meteorology*, 103(3), 279-300.
- 463 Von Randow, C., Manzi, A., Kruijt, B., De Oliveira, P., Zanchi, F., Silva, R., . . . Waterloo, M. (2004).  
464 Comparative measurements and seasonal variations in energy and carbon exchange over forest and pasture in  
465 south west amazonia. *Theoretical and Applied Climatology*, 78(1-3), 5-26.
- 466
- 467 Were, A., et al. (2007). "Analysis of effective resistance calculation methods and their effect on modelling  
468 evapotranspiration in two different patches of vegetation in semi-arid SE Spain." *Hydrology and Earth System*  
469 *Sciences Discussions* 11(5): 1529-1542.
- 470 Wilczak, J. M., Oncley, S. P., & Stage, S. A. (2001). Sonic anemometer tilt correction algorithms. *Boundary-*  
471 *Layer Meteorology*, 99(1), 127-150.
- 472 Williams, C. A., Hanan, N., Scholes, R. J., & Kutsch, W. (2009). Complexity in water and carbon dioxide fluxes  
473 following rain pulses in an african savanna. *Oecologia*, 161(3), 469-480.
- 474 Wilson, K., Goldstein, A., Falge, E., Aubinet, M., Baldocchi, D., Berbigier, P., . . . Field, C. (2002). Energy  
475 balance closure at FLUXNET sites. *Agricultural and Forest Meteorology*, 113(1), 223-243.
- 476 Xin, X., & Liu, Q. (2010). The two-layer surface energy balance parameterization scheme (TSEBPS) for  
477 estimation of land surface heat fluxes. *Hydrology and Earth System Sciences*, 14(3), 491-504.
- 478 Yuling, F. (2005). Energy balance closure at ChinaFLUX sites.
- 479
- 480



481 **Table 1: Measurements taken and instruments used at Skukuza flux tower**

Instrument	Model/ brand	Measurement
Sonic anemometer	Gill Instruments Solent R3, Hampshire, England	3-dimensional, orthogonal components of velocity (u, v, w (ms <sup>-1</sup> ))
Closed path gas analyser	IRGA, LiCOR 6262, LiCOR, Lincoln	Water vapor, carbon dioxide concentrations
Radiometer	Kipp and Zonen CNR1, Delft, The Netherlands	Incoming and outgoing longwave and shortwave radiation
HFT3 plates	Campbell Scientific	Soil heat flux at 5 cm depth with 3 replicates, i.e. two under tree canopies and one on open space
Frequency domain reflectometry probes	Campbell Scientific CS615, Logan, Utah	Volumetric soil moisture content with two in the clayey Acacia – dominated soils downhill of the tower at 3, 7, 16, 30, and 50 cm, and another two at 5, 13, 29, and 61 cm in the sandier Combretum – dominated soils uphill

482  
483

484

485 **Table 2: Statistical summary of annual values of the energy balance components**

Year	% data completion		H	LE	G	Rn
2000	14.16	Max	470.31	422.89	191.53	817.60
		Min	-139.77	-72.43	-61.60	-95.93
		Mean	45.82	36.11	5.32	91.46
2001	12.78	Max	790.82	513.09	292.87	899.90
		Min	-159.87	-85.95	-90.27	-116.58
		Mean	58.56	43.68	9.27	128.27
2002	17.77	Max	415.93	174.07	171.93	583.30
		Min	-117.66	-89.16	-86.00	-122.21
		Mean	61.35	10.29	4.10	90.72
2003	41.50	Max	556.21	308.71	217.60	879.30
		Min	-92.99	-97.81	-106.23	-116.04
		Mean	58.15	21.68	6.17	94.53
2004	28.21	Max	505.36	498.10	129.96	925.30
		Min	-150.08	-89.07	-69.76	-5.88
		Mean	56.46	17.99	7.97	156.10
2005	35.37	Max	606.28	737.43	288.20	933.20
		Min	-130.40	-97.00	-107.37	-4.92
		Mean	51.43	17.82	0.99	159.09
2006	7.59	Max	583.66	331.25	335.30	1003.30
		Min	-72.45	-119.09	-72.80	-6.56
		Mean	84.67	35.94	19.69	247.70
2007	48.77	Max	552.93	426.34	340.67	1011.30
		Min	-131.40	-130.79	-129.70	-6.71
		Mean	59.04	14.32	4.14	169.84
2008	54.30	Max	616.43	439.76	238.57	1038.50
		Min	-140.13	-144.97	-104.60	-5.91
		Mean	63.06	26.30	6.22	191.26
2009	42.69	Max	551.34	776.62	328.93	1060.50
		Min	-96.68	-135.43	-94.20	-155.90
		Mean	55.42	96.54	6.87	207.77
2010	57.65	Max	626.68	624.38	199.33	888.00
		Min	-173.11	-135.62	-66.35	-180.70
		Mean	57.23	52.54	3.74	105.10
2011	41.34	Max	591.16	688.46	171.27	832.00
		Min	-135.77	-127.02	-58.59	-96.50
		Mean	63.88	73.11	1.75	127.94
2012	27.62	Max	572.11	566.88	185.80	899.00
		Min	-171.83	-148.49	-50.92	-99.69
		Mean	59.25	52.49	2.16	111.31
2013	3.25	Max	317.98	661.09	79.67	742.05
		Min	-62.96	-27.19	-30.49	-90.30
		Mean	1.79	34.08	-15.64	-6.09
2014	28.66	Max	533.46	726.31	89.50	893.00
		Min	-238.65	-134.39	-33.36	-89.70
		Mean	59.37	69.55	1.18	147.30

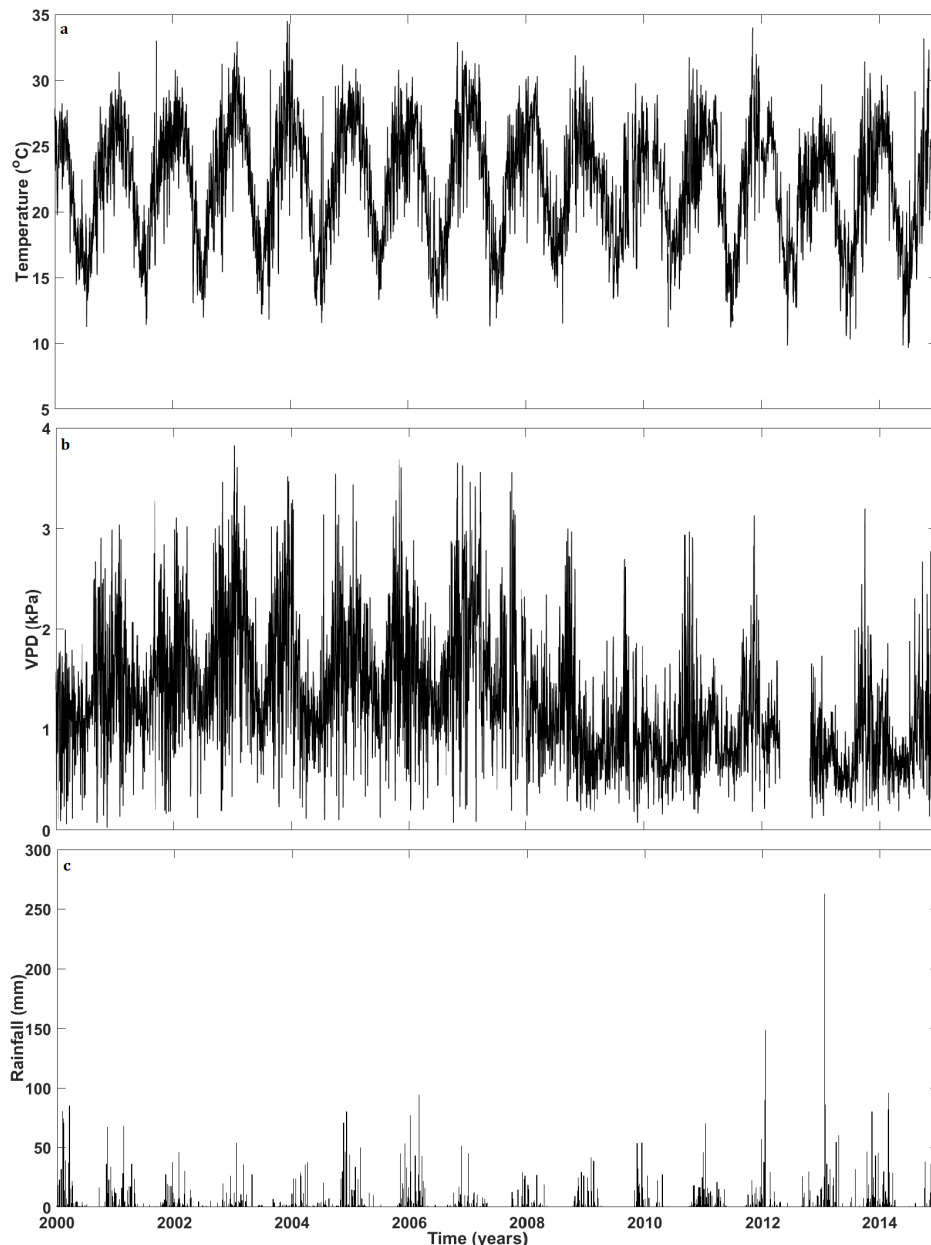
486  
487



488 **Figures**

489

490 **Figures**

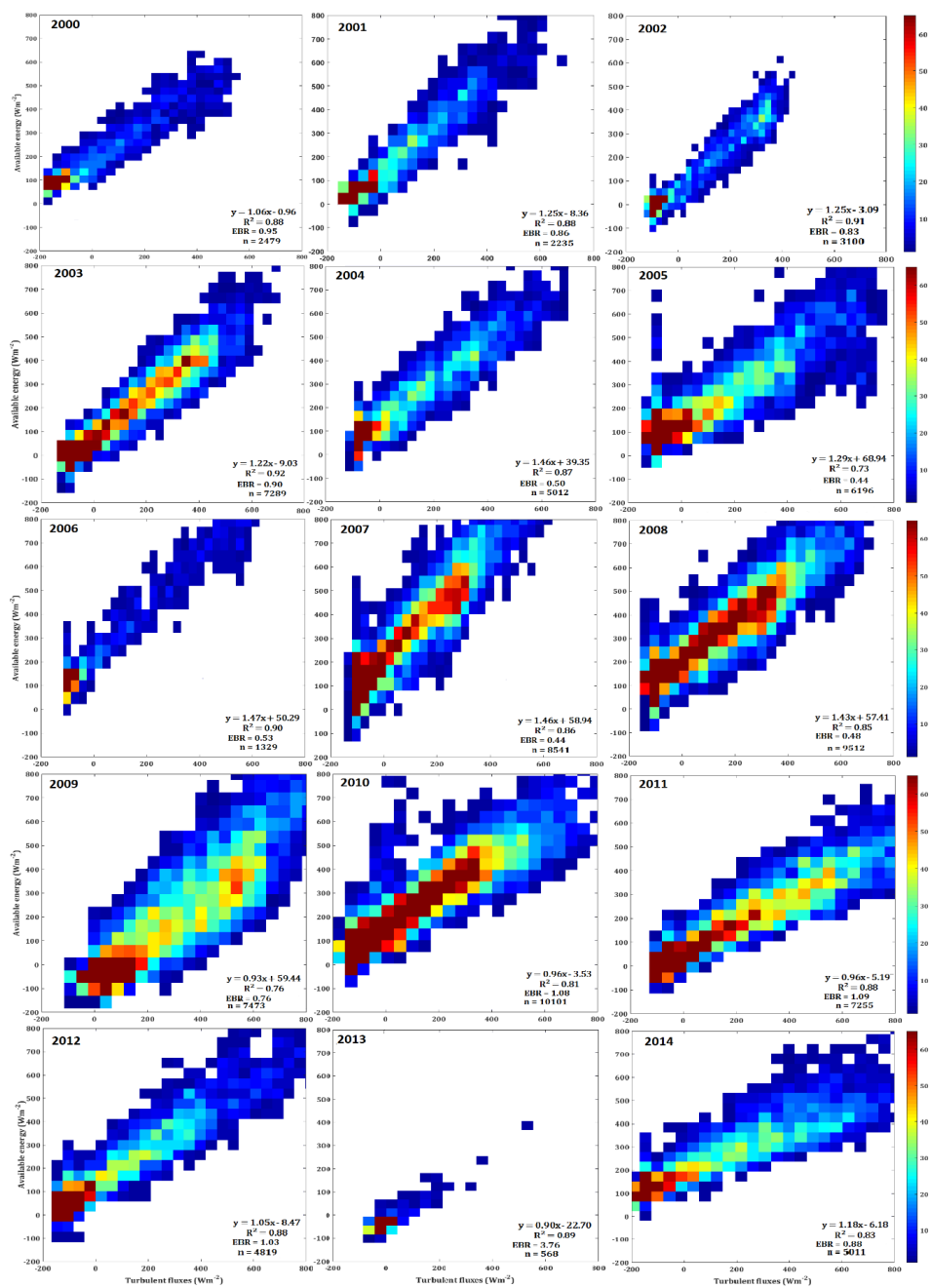


491

492

Figure 1: summaries of daily (a) average air temperature, (b) average VPD, and (c) total rainfall from 2000 to 2014

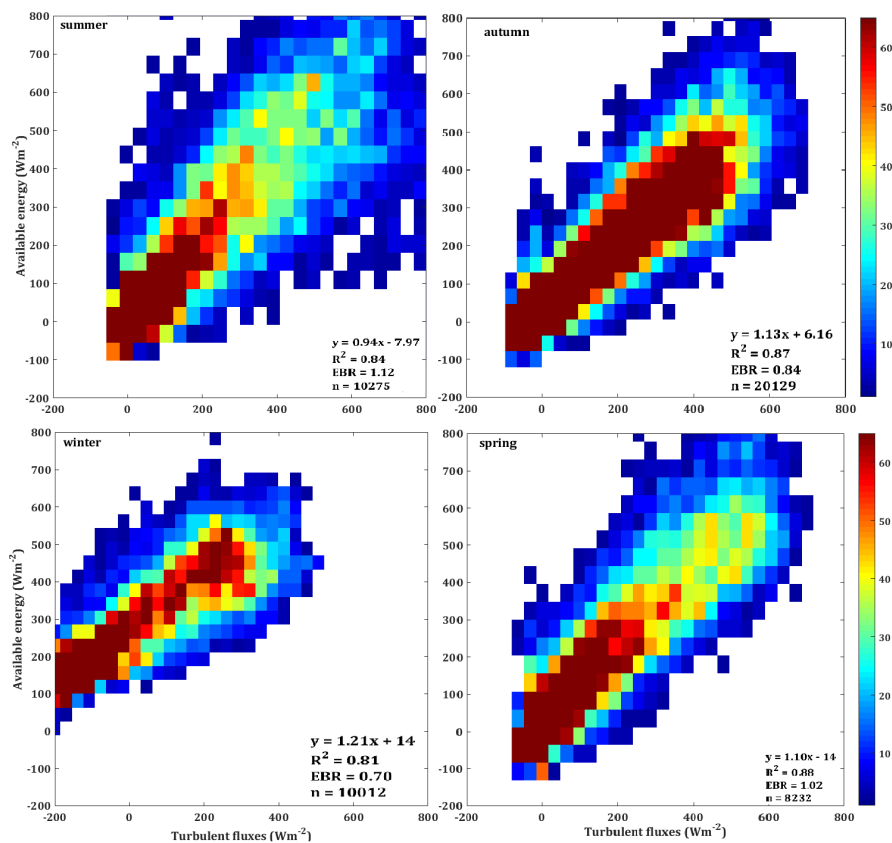
493



494  
 495  
 496  
 497  
 498

Figure 2: 15-year series of annual regression analysis of turbulent (sensible and latent) heat fluxes against available energy (net radiation minus ground conduction heat) from 2000 to 2014 at Skukuza, (SA). The colour bars represent the count of EBR values.

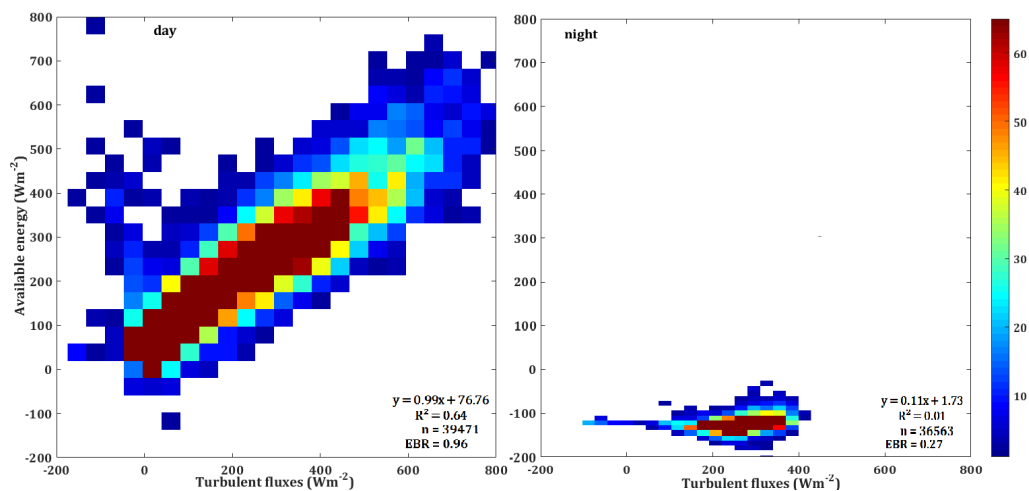




499

500 **Figure 3: Seasonal turbulent fluxes (H+LE) correlation to available energy (Rn-G) for Skukuza flux tower from**  
 501 **summer(Dec-Feb), autumn (March-May), winter (June-Aug), spring (Sept-Nov). The colour bars represent the count**  
 502 **of EBR values**

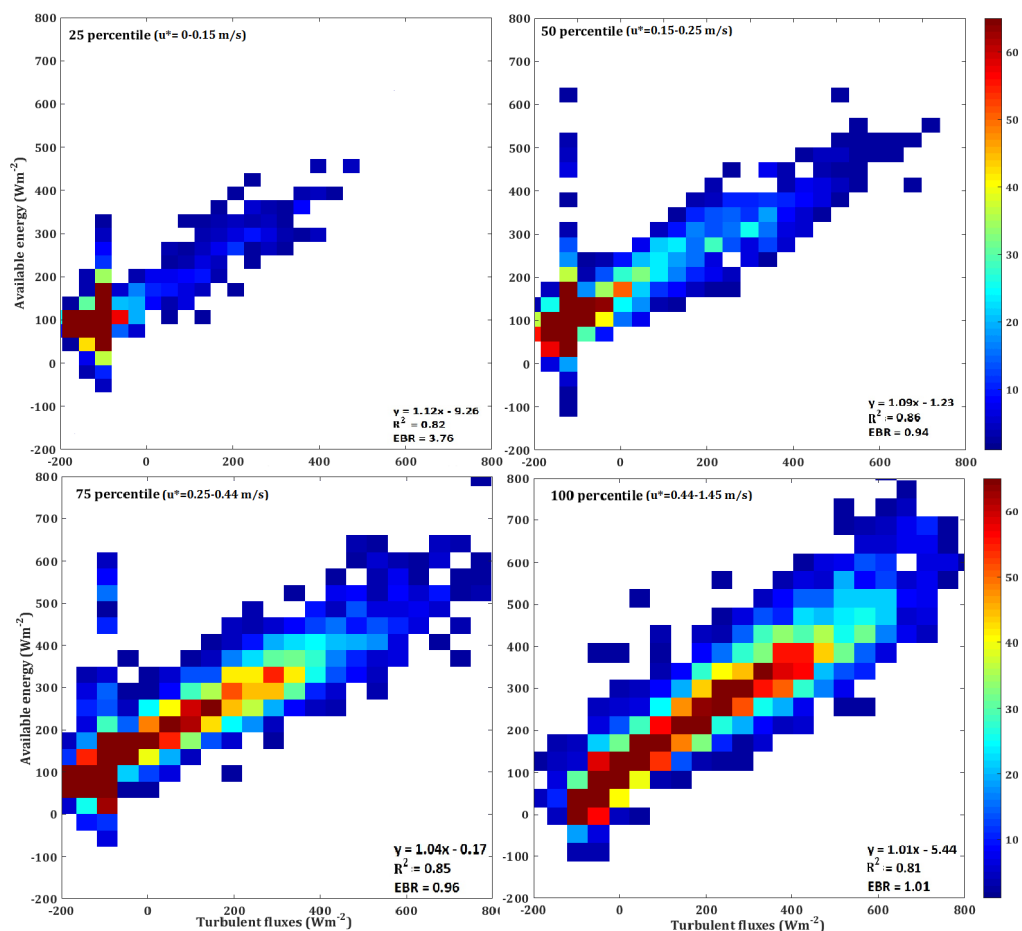
503



504  
505 **Figure 4: Turbulent fluxes correlation to available energy for daytime (a) and night-time (b), using the full (2000-2014)**  
506 **15-year available data series. The colour bars represent the count of EBR values**

507

508

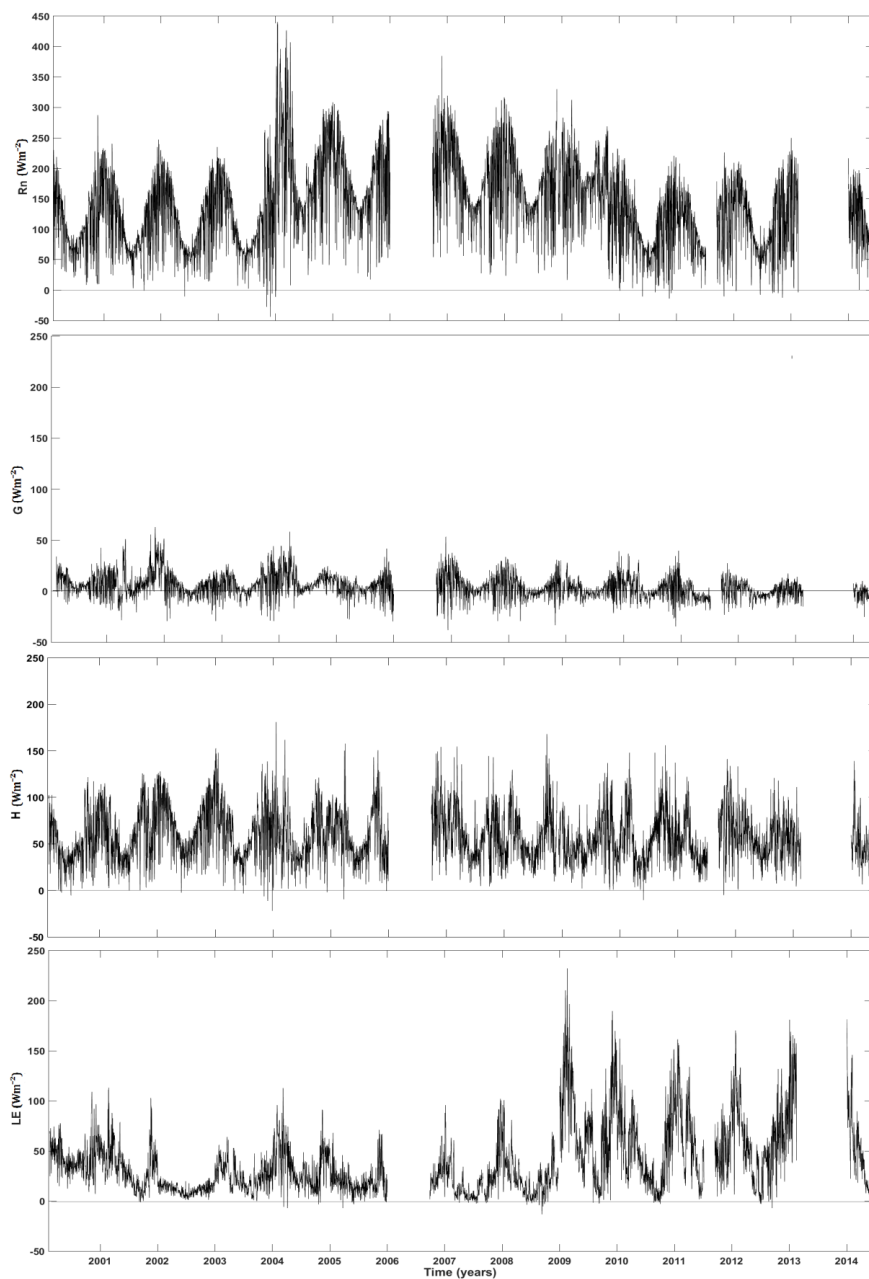


509  
 510 **Figure 5: OLS and EBR evaluations at different friction velocity sorted at 4 quartiles. The colour bar represents the**  
 511 **count of EBR values. The colour bars represent the count of EBR values.**

512

513

514

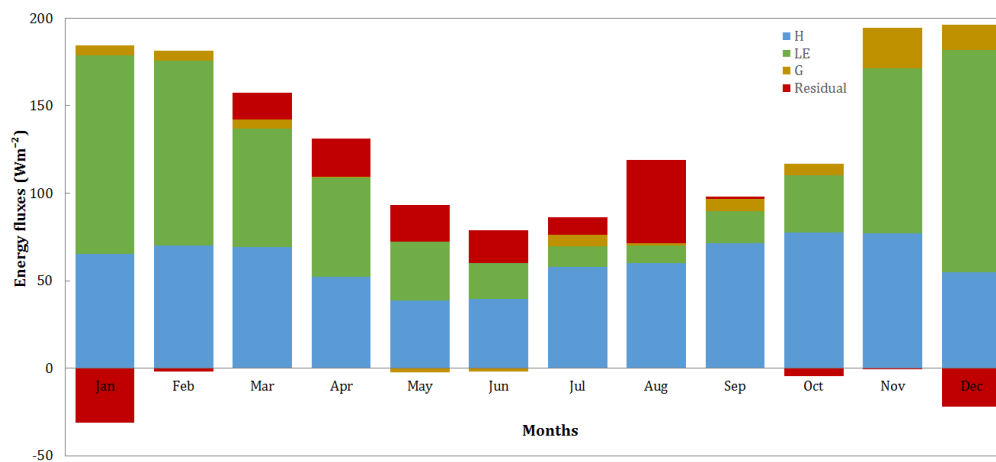


515  
516  
517  
518

Figure 6: Time series of daily mean surface energy balance component fluxes from 2000 to 2014 at Skukuza flux tower site (SA)

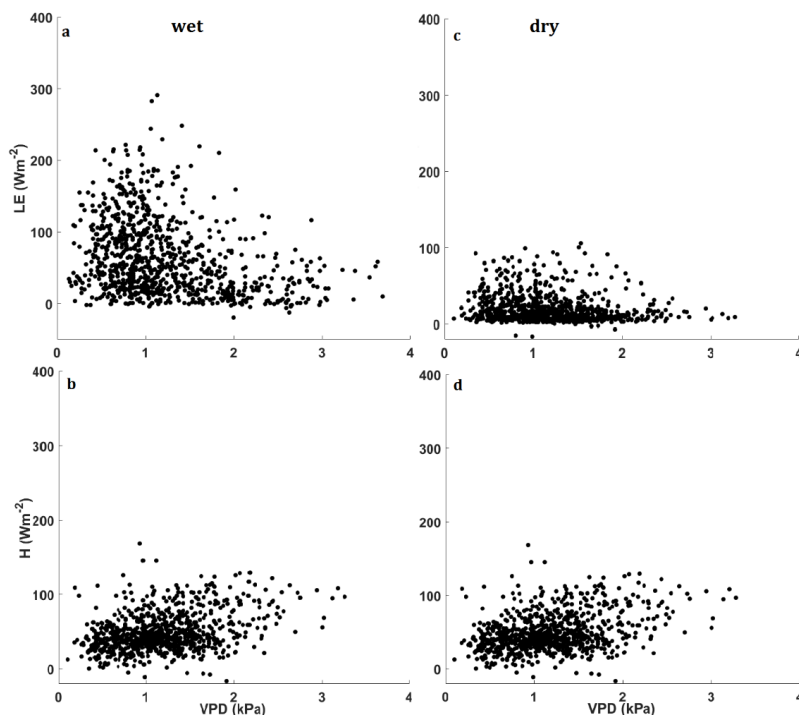


519



520  
521  
522  
523

Figure 7: 15-year (2000-2014) monthly means of surface energy balance fluxes of Skukuza flux tower site (SA), highlighting the partitioning of Rn

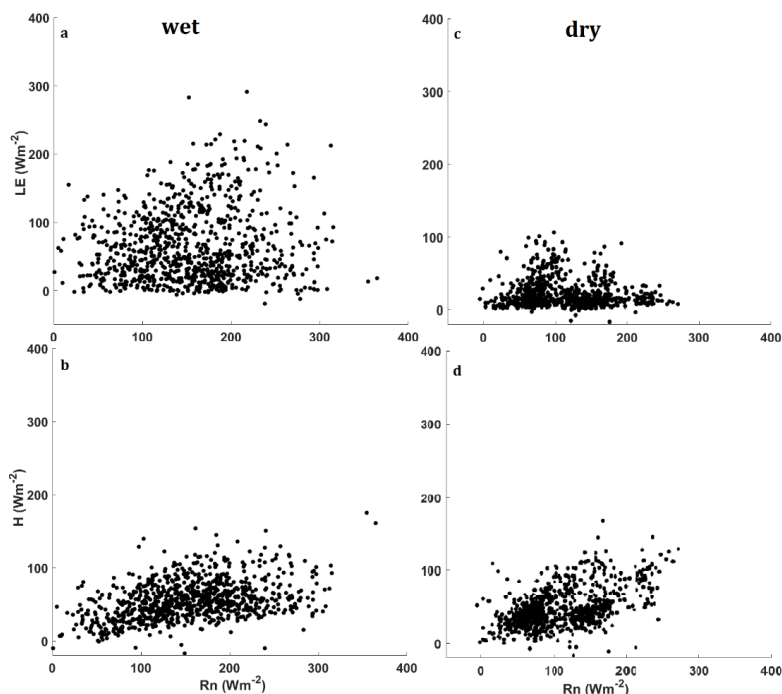


524

525

Figure 8: Relationship between the fluxes and VPD under wet and dry conditions

526



527  
528

Figure 9: Effects of net radiation on LE and H under wet and dry conditions